Chem

CellPress

Article

Diindenoanthracene Diradicaloids Enable Rational, Incremental Tuning of Their Singlet-Triplet Energy Gaps

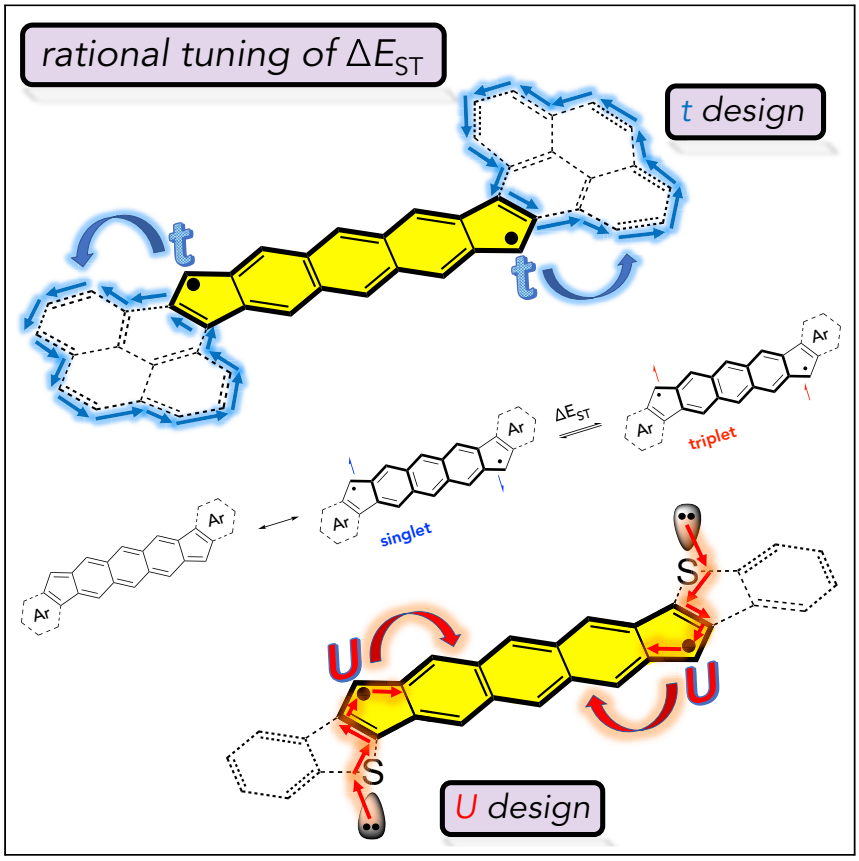

Haley and co-workers report the synthesis and physical characterization of a family of diradicaloids on the basis of the diindenoanthracene framework. Computations suggested that altering the external fused rings on both sides of the pentacyclic core would yield systematic changes in their open-shell properties, results that have been corroborated experimentally. This structure refinement approach provides a deeper understanding on how to tune the intrinsic properties of diradicaloid compounds in a rational and predictable manner.

Justin J. Dressler, Abel Cárdenas Valdivia, Ryohei Kishi, ..., Masayoshi Nakano, Juan Casado, Michael M. Haley

mnaka@cheng.es.osaka-u.ac.jp (M.N.)
casado@uma.es (J.C.)
haley@uoregon.edu (M.M.H.)

HIGHLIGHTS

A family of diradicaloid structures composed of nine fused rings was prepared

Systematic structural variation leads to rational changes in diradical character

Fine-tuning of the singlet-triplet energy gap to within a narrow 1.6 kcal mol^{-1} range

Dressler et al., Chem 6, 1353–1368
June 11, 2020
https://doi.org/10.1016/j.chempr.2020.02.010

Chem

CellPress

Article

Diindenoanthracene Diradicaloids Enable Rational, Incremental Tuning of Their Singlet-Triplet Energy Gaps

Justin J. Dressler,[1] Abel Cárdenas Valdivia,[2] Ryohei Kishi,[3] Gabriel E. Rudebusch,[1] Austin M. Ventura,[1] Brian E. Chastain,[1] Carlos J. Gómez-García,[4] Lev N. Zakharov,[5] Masayoshi Nakano,[3,6,7,8,*] Juan Casado,[2,*] and Michael M. Haley[1,9,10,*]

SUMMARY

A fundamental understanding of the inherent electronic and magnetic properties of open-shell diradicaloids is essential so that these properties can be modified to create molecules that meet the potential needs of industry. However, there have been very few attempts to date to systematically accomplish this in diradicaloid compounds. Here, we present the synthetic, spectroscopic, and computational investigation of a series of molecules based on the diindeno[1,2-*b*:1′,2′-*g*]anthracene framework. Calculations suggest that by altering the transfer integral term, t_{ab}, we are able to manipulate the diradical character and, thus, ΔE_{ST} within this series of molecules. Experimentally determined values by superconducting quantum interference device (SQUID) magnetometry show that we can effectively "tune" ΔE_{ST} of the five derivatives within a narrow 1.6 kcal mol^{-1} range.

INTRODUCTION

Interest in polycyclic aromatic hydrocarbons (PAHs) possessing diradical character has undergone a strong resurgence in recent years. The increase in reports of carbon-based diradicaloids has been fueled by both the inherent novelty of these molecules as well as their promise as organic electronic and magnetic materials.[1] Because of the different magnetic states that these molecules can possess, diradicaloid hydrocarbons have been posited to be useful in applications, such as molecular electronics and spintronics,[2] lithium-ion batteries,[3] nonlinear optics,[4–7] and singlet fission.[8–10] To date, however, their application still remains to be realized, though there have been some preliminary attempts.[7,11,12] Since the first reports of carbon-centered diradicaloids, namely Thiele's hydrocarbon (**1**, Figure 1A) in 1904[13] and Tschitschibabin's hydrocarbon (**2**) in 1907,[14] the study of this broad class of compounds has offered new insights on the fundamental nature of the π bond, as well as on unusual electronic and magnetic properties in π-expanded systems.[15] The desire to explore this chemical space and fully understand these molecules has led to the synthesis of many classes of organic diradicaloids (Figure 1B), including but not limited to bisphenalenyls (**3**),[16–19] extended quinodimethanes (**4**),[20–22] indenofluorenes[23–26] and related diindenoacenes (**5**),[26–33] zethrenes (**6**),[33–37] anthenes (**7**),[38,39] and higher-order acenes (**8**).[40–42] Arguably the biggest challenge in discovering new diradicaloid PAHs, and thereby limiting our understanding of this class of compounds, is that the diradical character that makes these systems potentially interesting also makes their synthesis demanding. As shown in Figure 1B, strategic placement of large steric protecting groups near the areas of

The Bigger Picture

The study of diradicaloid (open-shell) molecules offers new insights into the fundamental nature of the π-electron bond as well as new avenues of research regarding chemical reactivity and unusual electronic and/or magnetic properties in π-expanded systems. Although literature has recently seen an increase in the number of new diradicaloids, there are a few cases in which structural modification is made to the original scaffold to modify these properties. If the posited materials applications for organic diradicaloids are to come to fruition, the ability to incrementally and rationally change molecule properties while maintaining stability will be essential. Here, we show how to design new diradicaloids by tuning the transfer integral term, t_{ab}. This series of compounds maintain the same 2,6-anthraceno π-conjugation of the quinoidal-diradical core, with only minor alteration to the molecular geometry, thus following an approach based on structure refinement.

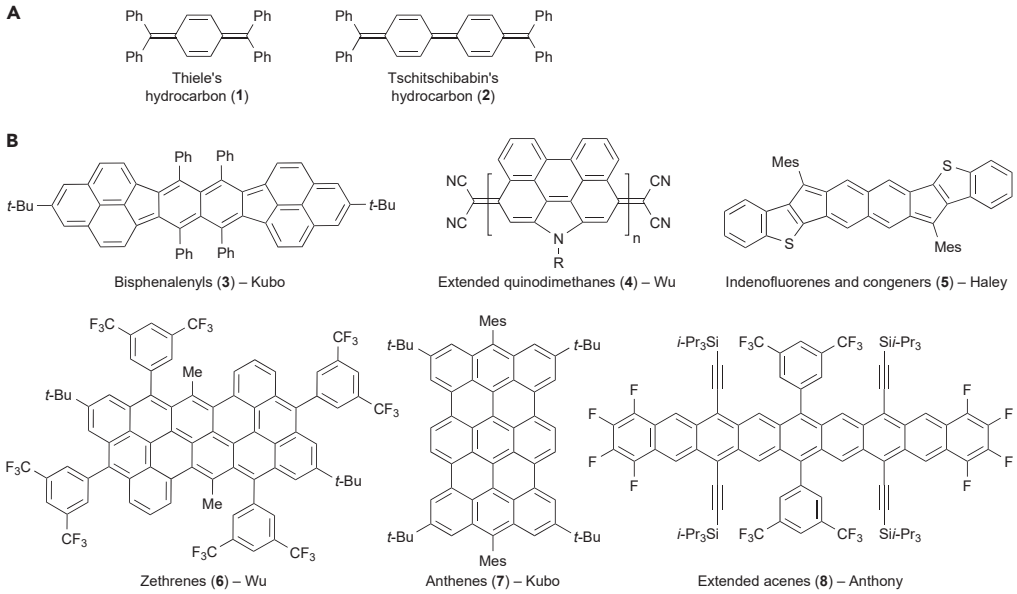

Figure 1. Examples of Known Diradicaloid Molecules

(A) The first two reported carbon-centered diradicaloids in the literature, Theile's (**1**) and Tschitschibabin's (**2**) hydrocarbons, drawn in the closed-shell resonance form.

(B) Representative examples of recently reported diradicaloids (**3**–**8**), drawn in the closed-shell resonance form (Mes, 2,4,6-trimethylphenyl).

high radical density permits more stable derivatives to be characterized successfully. Diradicaloid molecules exhibit a number of less common properties,[43–45] such as a narrow highest occupied molecular orbital-lowest occupied molecular orbital (HOMO-LUMO) energy gap,[1] low-energy electronic absorptions attributable to a low-lying doubly excited electronic configuration,[46,47] multicenter bonding,[16,17] redox amphoterism,[19,28] electron spin resonance (ESR) signal(s), and peak broadening in the proton NMR spectrum.[48]

To date, two basic strategies have been used in diradicaloid PAHs to modify the diradical character index (y) and its closely related observable property, the singlet-triplet energy gap (ΔE_{ST}):[1] (1) altering the length of the π-conjugated core[21,30,34,38,43] or (2) varying the orientation of the radical centers attached to the core.[23–25,36,49] Although logical series of diradicaloid scaffolds have been reported that rely on one of these two strategies to modulate such properties, the observed variations were often large in magnitude and did not lead to the ability to fine-tune ΔE_{ST} and *y* in a precise way. The study closest to accomplishing a fine-tuning of ΔE_{ST} was an elegant series of oligorylene ribbons, reported by Wu in 2017 with four derivatives within a 2.0 kcal mol^{-1} range;[50] however, the work did not provide insight as to what electronic factors were being affected, and there was only modest agreement between the experimental ΔE_{ST} and the calculated values along with limited stability of the longer oligomers. Although concepts such as aromaticity recovery and number of Clar sextets as well as molecule twisting and nonplanarity provide a straightforward way to qualitatively interpret open-shell structures, a fundamental quantitative knowledge of how to manipulate the underlying physical properties that affect diradical character is lacking. To that end, we sought to rationally design molecules with finely tuned diradical character *y* on the basis of the two fundamental quantum chemical quantities that control it,[51] namely, an electron-electron repulsion term (*U*) and an energy resonance term or transfer integral (t_{ab}) that gives account of the electron delocalization. As noted in a recent publication,

[1]Department of Chemistry & Biochemistry and the Materials Science Institute, University of Oregon, Eugene, OR 97403-1253, USA

[2]Department of Physical Chemistry, University of Malaga, Campus de Teatinos, s/n, 29071 Malaga, Spain

[3]Department of Materials Engineering Science, Graduate School of Engineering Science, Osaka University, Toyonaka, Osaka 560-8531, Japan

[4]Department of Inorganic Chemistry and Instituto de Ciencia Molecular, Universidad de Valencia, C/José Beltrán 2, 46980 Paterna, Spain

[5]CAMCOR, University of Oregon, Eugene, OR 97403-1433, USA

[6]Quantum Information and Quantum Biology Division, Institute for Open and Transdisciplinary Research Initiatives, Osaka University, Toyonaka, Osaka 560-8531, Japan

[7]Center for Spintronics Research Network (CSRN), Graduate School of Engineering Science, Osaka University, Toyonaka, Osaka 560-8531, Japan

[8]Institute for Molecular Science, 38 Nishigo-Naka, Myodaiji, Okazaki 444-8585, Japan

[9]Phil and Penny Knight Campus for Accelerating Scientific Impact, University of Oregon, Eugene, OR 97403-6231, USA

[10]Lead Contact

*Correspondence: mnaka@cheng.es.osaka-u.ac.jp (M.N.), casado@uma.es (J.C.), haley@uoregon.edu (M.M.H.)

https://doi.org/10.1016/j.chempr.2020.02.010

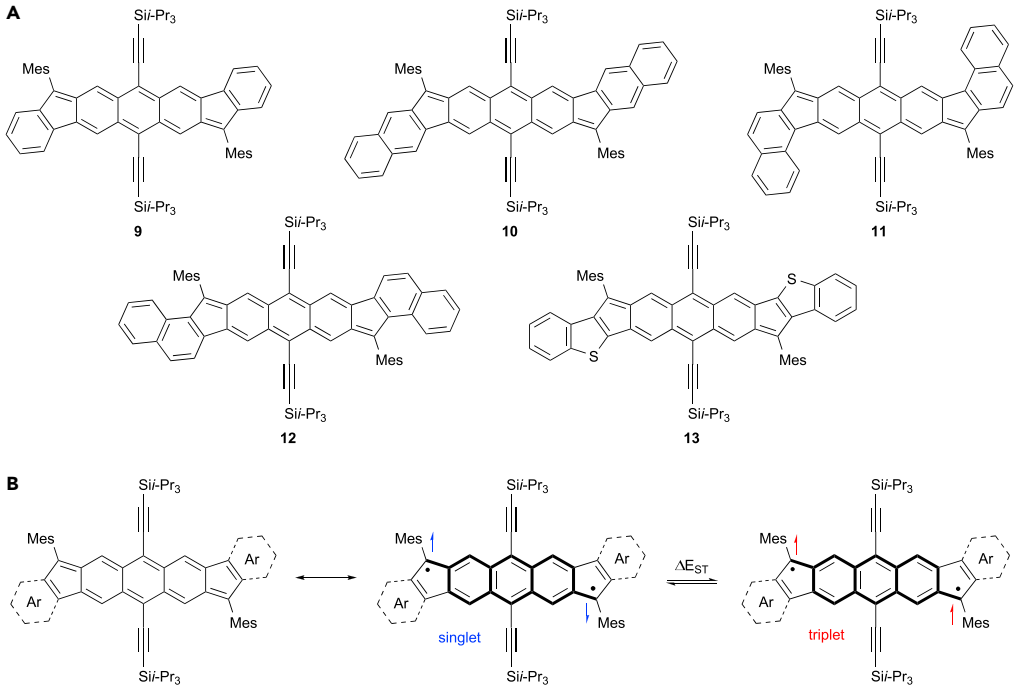

Figure 2. Diradicaloid Molecules Based on the Diindeno[1,2-*b*:1′,2′-*g*]anthracene Scaffold

(A) Target DIAn compounds **9**–**13** illustrate how incremental changes to the diradical scaffold can result in significant changes to the overall magnetic properties of each molecule.

(B) Closed-shell (left), open-shell singlet (center), and open-shell triplet (right) forms of a DIAn derivative with generic fused aryl groups; the 2,6-anthraceno conjugation of the two radical centers is shown by the bolded bonds.

"The ability to tune the S–T gap would provide materials based on diradicaloid hydrocarbons with accessible bulk magnetic moments and therefore plays a central role in design of materials with conducting and magnetic properties."[46]

Although the global analysis of the electronic structure of diradicals is contained in the U versus t_{ab} balance, an experimental local parameter directly connected with the diradical character is the bond order (BO) of the outer rings fused to the indacene core. In 2016, we reported a series of indeno[1,2-*b*]fluorenes, where the change of BO dramatically affected the strength of the paratropicity within the indacene core.[52] Whereas benzothiophene fusion (BO = 2) afforded compounds that were nearly as antiaromatic as *s*-indacene itself,[29] linear fusion of anthracene (BO = 1.25) quenched indacene paratropicity.[32] Given the known relationship between antiaromaticity and diradical character,[45,53] we hypothesize that using the same BO alteration strategy within the diindeno[1,2-*b*:1′,2′-*g*]anthracene scaffold (DIAn, **9**; Figure 2A), a stable molecule with significant diradicaloid character,[27] would allow us to craft a series of structurally similar molecules (**10**–**13**; Figure 2A). This "structure refinement approach," based on subtle alteration of molecular geometry yet with retention of the same 2,6-anthraceno π-conjugated quinoidal-diradical core (Figure 2B), would enable a systematic, quantitative study examining incremental change in the diradical character y, the ΔE_{ST} energy gap, and the overall electronic properties of a closely related series of stable diradicaloids. We recently reported that thiophene isomerism in derivatives of **5** permits rational modification of the repulsion term U and, thus, a ~1 kcal mol^{-1} change in ΔE_{ST}.[54] Herein, we disclose the preparation of DIAn derivatives **10**–**13** as well as a new synthesis of **9** and examine the trend of systematically increasing diradical behavior by variable

Table 1. Theoretical Calculations and Physical Parameters for the Model Compounds 9′–13′

Compound[a]	9′	10′	11′	12′	13′
Experimental ΔE_{ST} [kcal mol^{-1}]	−4.2	−4.8	−3.8	−3.2	−3.4
Adiabatic ΔE_{ST} (+ZPVE) [kcal mol^{-1}] [b]	−4.71	−5.09	−4.16	−3.45	−3.41
y (PUHF) [–][c]	0.623	0.638	0.686	0.711	0.815
y (CASCI) [–] [d]	0.213	0.198	0.235	0.250	0.298
$\|t_{ab}\|$ [eV] [d]	0.916	0.905	0.818	0.781	0.774
$U/2 = K^{M}_{gu}$[eV] [d]	1.435	1.348	1.378	1.377	1.572
$(U/2)f_{ST}(y)$ [eV] [d]	–0.891	–0.909	–0.762	–0.706	–0.635
$2K_{ab}$ [eV] [d]	1.435	0.041	0.087	0.096	1.572

[a]For computational efficiency, $SiMe_3$ used in place of Si*i*-Pr_3.
[b]Calculated by using the spin-flip non-collinear time-dependent density functional theory (SF-NC-TDDFT) with the PBE50 functional and 6–311G* basis set. Geometry optimization followed by the frequency analysis and the zero-point vibrational energy (ZPVE) estimation for the singlet and triplet states were performed at the R and UB3LYP/6-311G* level, respectively.
[c]Calculated at the PUHF/6–311G* level.
[d]Estimated at the CASCI(2,2)/6–311G* level by using the Kohn-Sham orbitals at the tuned-LC-RBLYP/6–311G* where the range-separating parameter was tuned for each system by using the "IP-tuning" scheme.

temperature NMR and Raman spectroscopy, electronic absorbance spectroscopy, and bond length analysis of their solid-state structures. Additionally, in our continuing efforts toward fine-tuning the ΔE_{ST} energy gap in new diradicaloids and in the interest of full understanding of the molecular and electronic-based reasons of such a tuning, we probe ΔE_{ST} experimentally utilizing superconducting quantum interference device (SQUID) magnetometry. In conjunction, quantum chemical calculations are used to rationalize the key electronic factors that lead to such modulation, i.e., the transfer integral t_{ab}.

RESULTS AND DISCUSSION

Calculations

To corroborate the "local" BO hypothesis as well as the "global" U versus t_{ab} fine balance in the definition of the diradical properties, quantum chemical calculations on model structures **9′–13′** were performed, both without (Table S1) and with the two (trialkylsilyl)ethynyl groups (Table S2). The relevant theoretical diradical index values (y, that takes values of "0" or pure closed-shell molecules and "1" for pure diradicals) calculated at the spin-projected (P)UHF/6–311G* level, together with the ΔE_{ST} gaps at the spin-flip time-dependent density functional theory (SF-TDDFT)[55,56] level are given in Table 1, along with the experimental ΔE_{ST} values (see also Figures S23 and S24). A nice correspondence between the experimental and theoretical ΔE_{ST} gaps is observed, which allows us to use the 2 electrons in the 2-site model of diradicals to obtain the main physical parameters (also shown in Table 1) dictating their unique diradical structures at the CASCI(2,2)/6–311G* level using the tuned-LC-RBLYP Kohn-Sham orbitals.[57,58] Note that even though the y and ΔE_{ST} values by the two-electron model tend to under- and over-estimate the results at the spin-projected unrestricted Hartree-Fock (PUHF) and SF-TDDFT levels, respectively, the trends of the results by benzo-fusion are well reproduced. These values are all condensed in Equations 1 and 2 of this model:

$$y = 1 - \frac{1}{\sqrt{1 + (4t)^{-2}}} = 1 - \frac{1}{\sqrt{1 + \left(\frac{U}{4t_{ab}}\right)^{2}}} \qquad \text{(Equation 1)}$$

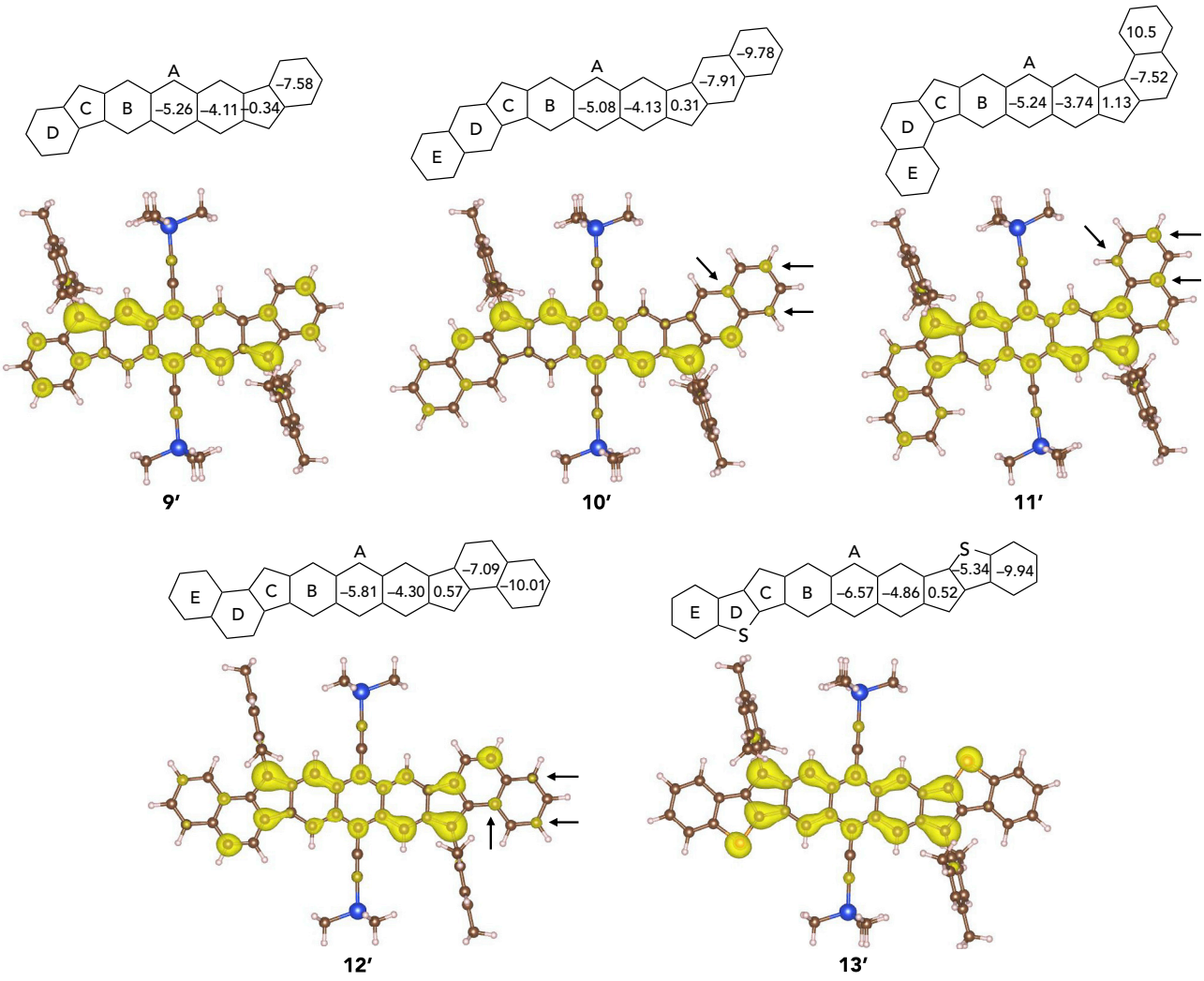

Figure 3. Odd Electron Density Maps and NICS(1) Values of Models 9′–13′

Odd electron densities were calculated at the tuned-LC-RBLYP CASCI(2,2)/6–311G* level. Magnetic response calculations were performed at the LC-UBLYP/6–311G* level where the same range-separating parameters as those for the estimation of physical parameters were employed (for details, see Supplemental Information). Yellow surface of odd electron density map represents the isosurface with the contour value of 0.0005 a.u. NICS(1) values are in ppm.

$$\Delta E_{ST} = 2K_{ab} + \frac{U}{2}\left(1 - \sqrt{\frac{1}{y(2-y)}}\right) = 2K_{ab} + \frac{U}{2}f_{ST}(y) \qquad \text{(Equation 2)}$$

Here, K_{ab} indicates a direct exchange integral. The increase of the chain length from DIAn (**9′**) to dibenzoDIAns (**10′**, **11′**, and **12′**) always decreases t_{ab} (i.e., enhances delocalization over the terminal parts), which is seen by the appearance of odd-electron density partially delocalized into the terminal rings (i.e., arrows next to E rings in Figure 3; see Figure S35 for structural depiction of the possible resonance forms). The rationale for this is that the aromatic character of the outer benzenes in DIAn (rings D in Figure 3) is slightly stronger than in the equivalent benzenes in the angular-fused dibenzoDIAn derivatives, which is confirmed by the reduced amplitudes of the nucleus-independent chemical shift (NICS(1)) values in **11′** and **12′** in Figures 3 and S27. On the other hand, the NICS(1) value on ring D of **10′** is slightly larger than that in **9′**, which accounts for the smaller change in t_{ab} on **9′** → **10′**

than in 9′ → 11′ and 12′. From Equation 1, we see that smaller t_{ab}, such as in the case of dibenzoDIAns compared with DIAn, increases the diradical character in Table 1 because the change in U is relatively small (see the Supplemental Information for further discussion of integrals U and t). Finally, the evolution of the t_{ab} in the dibenzoDIAn series is also in agreement with the overall shift of the low-energy absorption bands of the UV-vis-NIR spectra of 9′ → 10′/11′/12′ (*vide infra*).

Additional fusion of a six-membered ring onto the bay region of rings C-D-E of 12′ gives rise to the known bisphenalenyl-fused anthracene derivative[18] (BPLA; its structure and computational data are given in Figure S28 and Table S3). Results for BPLA show a much smaller t_{ab} than 12′ (0.467 eV in BPLA versus 0.781 eV in 12′) and a larger diradical character y (0.883 in BPLA versus 0.711 in 12′ at the PUHF level), highlighting the effect of greater delocalization of the odd-electron density (Figures S29–S32) in the terminal rings and reduced aromaticity in the common benzenes in BPLA (−5.30/−7.65 ppm in BPLA versus −7.09/−10.01 ppm in 12′).

The inter-site repulsion term U, the other key electronic factor, decreases from 9′ → 10′/11′/12′, but the magnitude of this change is smaller than that in t_{ab}, which results in the increase of y as explained above. However, U, conversely to t_{ab}, increases on 10′ → 11′/12′, which might indicate a better repulsion screening in the terminal moiety of 10′. Even though there is a balance between the $U/2$ and $f(y)$ in ΔE_{ST}, the reduction of U and t_{ab} for 9′ → 10′ results in a slight increase of the ΔE_{ST} as observed experimentally and predicted by calculations. Results of $U/2$ for 10′, 11′, and 12′ (1.348, 1.378, and 1.377 eV, respectively) are close to that of phenalenyl analog BPLA (1.385 eV), illustrating that the major change in the diradical features between the dibenzoDIAns and BPLA primarily comes from the role of t_{ab}.

For the PAHs under study, the t_{ab} term shows a greater variaiton from compound to compound than the U term, meaning that the two unpaired electrons are progressively less coupled or less bonded (indicating a larger degree of delocalization) on 10′ → 11′/12′ and is what primarily determines the variation of y and of the ΔE_{ST} gaps, although the results are determined by the subtle balance of several terms. Conversely, we have recently shown that y /ΔE_{ST} can be modulated by considering suitable chemical structures that mainly modify U keeping t_{ab} almost constant, for instance, by introducing sulfur atoms within the full PAH structure.[33,54] As a part of this study, compound 13 with a common anthracene core and terminal benzothiophene-based moieties is also reported. The molecule is isostructural with dibenzoDIAn 12, where the (CH=CH) motif opposite the apical carbon has been replaced with an isoelectronic S atom. In this case t_{ab} only slightly changes from 12′ (0.781 eV) to 13′ (0.774 eV), whereas $U/2$ significantly increases from 1.377 eV in 12′ to 1.572 eV in 13′ and, thus, justifies the larger diradical character (0.711 in 12′ and 0.815 in 13′) in spite of a similar ΔE_{ST} (calculated as −3.45 kcal mol^{-1} in 12′ and −3.41 kcal mol^{-1} in 13′), which is primarily due to the reduction of $U/2$ term.[54]

Synthesis

To prepare a family of modified DIAn derivatives, we sought a more modular synthetic route. As with the original preparation of 9, steric protection at the sites of high radical density with mesityl (2,4,6-trimethylphenyl) groups will kinetically shield the reactive sites, and the large mesityl and (triisopropylsilyl)ethynyl ((TIPS)ethynyl) groups should provide resistance to degradation pathways and enhance solubility. Starting from known dibromoanthracene 14[59] (Scheme 1A), selective deprotonation at the 3- and 7-positions by using lithium tetramethylpiperidide (LiTMP), followed by careful addition of gaseous CO_2, and then protonation with dilute aqueous acid

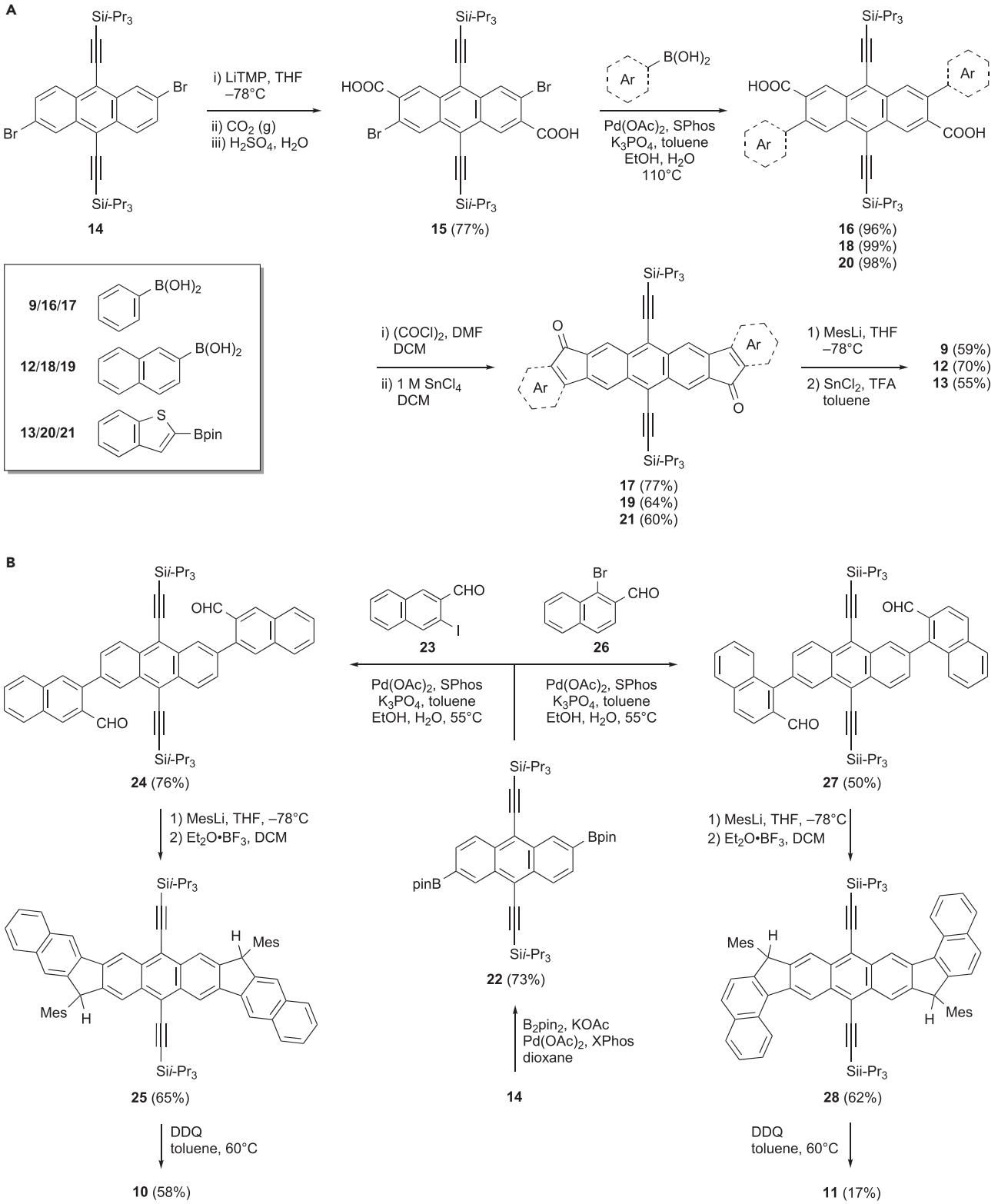

Scheme 1. Synthesis of Diindeno[1,2-*b*:1′,2′-*g*]anthracenes 9–13

(A) Friedel-Crafts acylation route to prepare **9**, **12**, and **13**, which has been successfully executed with the cross-coupling partners on the bottom left of the scheme.

(B) Friedel-Crafts alkylation route to prepare **10** and **11**.

afforded diacid **15** as the key intermediate to which a variety of aryl groups could be attached via Suzuki-Miyaura cross-coupling. Using DIAn itself as a test case, cross-coupling **15** with phenylboronic acid provided diaryldiacid **16** in 96% yield, which was subjected to Friedel-Crafts acylation conditions to form the heptacyclic core of DIAn-dione **17** in a very good yield (confirmed by X-ray analysis; see Figure S18). Nucleophilic attack on **17** by mesityllithium afforded the intermediate diol (not shown), which was then treated with $SnCl_2$ and catalytic trifluoroacetic acid (TFA) to furnish the fully conjugated core of DIAn **9**, whose spectral data were identical with those previously reported.[27] Repetition of this synthetic sequence using 2-naphthylboronic acid and benzothiophene 2-boronpinacolate ester[60] gave diacids **18** and **20**, respectively, that were converted into diones **19** and **21**, then ultimately into new DIAn derivatives **12** and **13** isolated as blue and blue-black solids, respectively.

Given the propensity of naphthalene to undergo electrophilic aromatic substitution at the 1/4/5/8-positions, the preparation of the *syn* and *linear* dibenzoDIAn derivatives required a return to the original DIAn synthetic route. Starting again from **14**, Pd-mediated double Miyaura borylation with B_2pin_2 afforded bis(boronate ester) **22** (Scheme 1B). Cross-coupling this molecule with two equivalents of iodoaldehyde **23** (see the Supplemental Information for its preparation) gave dialdehyde **24**, which was then reacted with excess MesLi followed by Friedel-Crafts alkylation using $BF_3{\cdot}OEt_2$ to furnish dihydroDIAn **25**. Oxidation with 2,3-Dichloro-5,6-dicyano-1,4-benzoquinone (DDQ) provided the *linear* dibenzoDIAn **10** as an emerald green solid in good overall yield. Repetition of this sequence using bromoaldehyde **26** gave dial **27**, which was turned into dihydro intermediate **28** and then *syn* dibenzoDIAn **11** (army green solid) in an analogous manner. As with the original synthesis of **9**, selective ring closure occurs exclusively at the C3 and C7 positions of the anthracene core as a result of the steric clash between the bulky mesityl and TIPS groups. Careful handling and storage of all the diarenoDIAn derivatives is required once synthesized as these molecules begin to degrade at room temperature if exposed to air for extended periods of time. Unlike the parent system **9**, which has a half-life in solution of 64 days,[27] the half-lives of the diarenoDIAns in solution range from ~20 days for **10** to as little as 4.5 days for **13** (Figures S12–S15); therefore, as the diradicaloid character of a molecule increases, its stability correspondingly decreases.

NMR Spectroscopy

To gather more evidence of the diradical nature of these compounds, variable temperature (VT) ^{1}H NMR spectroscopy was performed with each derivative. Typical of molecules with pronounced open-shell character, the aromatic region of the ^{1}H NMR spectra of **11**–**13** at room temperature showed either broad, unresolved peaks or a completely flat baseline, as illustrated for **12** in Figure 4 (see also Figures S1 and S4–S7). Cooling of the samples in the spectrometer did result in the appearance of discernable peaks around −15°C to −30°C with the peaks continuing to grow until the experimental cutoff of −55°C, where the aromatic signals never gain full resolution. Importantly, when the instrument was warmed back to room temperature, the new spectrum resembles the original room temperature spectrum, confirming that **11**–**13** do not undergo a reaction and/or decomposition during the VT NMR experiments. Attempts to obtain fully resolved spectra of a sample of **12** dissolved in THF-d_8 and cooled to −100°C were only modestly successful (Figures S2 and S3) as compound **12** was also less soluble in THF-d_8 than in $CDCl_3$.[61] Nonetheless, this experiment suggests that a thermally accessible, magnetically active species is responsible for broadening the aromatic signals and that even at −100°C the magnetic species is still somewhat populated, justifying the lack of full resolution.

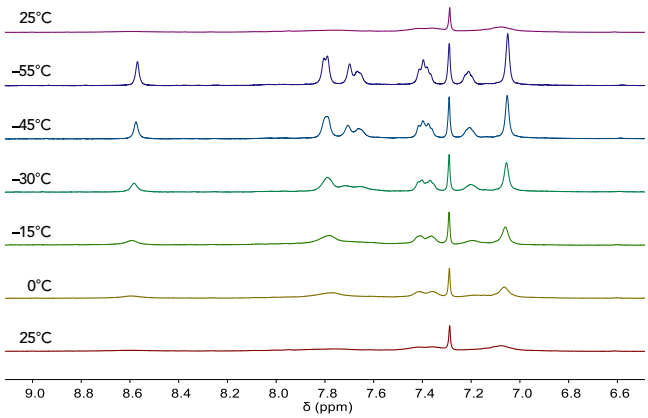

Figure 4. Variable Temperature NMR Spectroscopy Studies of 12

VT ^{1}H NMR spectra of the aromatic region of *anti*-dibenzoDIAn **12** in $CDCl_3$ showing thermal depopulation of the paramagnetic triplet state at low temperatures.

In contrast to **11**–**13**, the VT ^{1}H NMR spectra collected for *linear* dibenzoDIAn **10** exhibited very little to no peak broadening. At room temperature the aromatic region displayed relatively well-defined aromatic signals and cooling to −55°C resulted in full resolution of the aromatic signals, suggesting that the magnetic species was minimally populated at room temperature and below (Figures S8 and S9). Upon heating a $(CDCl_2)_2$ solution of **10** to 140°C, thermal broadening of the aromatic signals only began to occur at the experimental cutoff (Figures S10 and S11). The behavior of **10** in the high-temperature NMR experiments matches more closely to that of DIAn **9** (onset of broadening at 50°C),[27] with a higher onset point, indicative of the larger singlet-triplet energy gap that **10** possesses.

X-Ray Crystallography

To gain insight into the ground-state molecular structure of diradicaloid PAHs, single-crystal X-ray diffraction (XRD) and bond length analysis of the resultant structures have been used as a rough guideline to compare diradical character experimentally. Fortuitously, crystals that were suitable for XRD were grown by slow diffusion of CH_3CN into $CHCl_3$ for all four new DIAn derivatives and their structures secured (Figure 5). Similar to **9**, DIAns **10**–**13** are centrosymmetric. Molecules **10**, **12**, and **13** pack roughly as 1D stacks, whereas **11** appears like a 2D brickwork pattern (Figures S19–S22). There are no short C···C contacts (<3.8 Å) in the structures of **10** or **11**. DibenzoDIAn **12** contains two close C···C contacts (∼3.45 Å) between ring D and the same ring of its nearest neighbor. Compound **13** has close C···C (3.43 Å) and C···S contacts (3.53 Å), also between neighboring D rings. These distances are considerably longer than those for Kubo's related bisphenalenyl-fused arenes (3.1–3.2 Å), which exhibit strong π-dimer formation in the solid state;[16,17] thus, the likelihood of magnetic interactions between neighboring molecules of **12** and **13** in the solid state is minimal.

The outer naphthalene units of compounds **10**–**12** have bond lengths typical of a naphthalene motif, pointing to the aromatic character of the outer rings (also supported by the NICS(1) calculations). For benzothiophene-fused **13**, there is a distinct asymmetry in the C–S bond lengths (1.717 and 1.761 Å), similar to what was found for **5** (1.716 and 1.760 Å), which is due to the increased conjugation from the linear arrangement of the anti-fused S atom to the radical center versus a cross-conjugation arrangement if the thiophene was fused in a *syn*-fashion.[54]

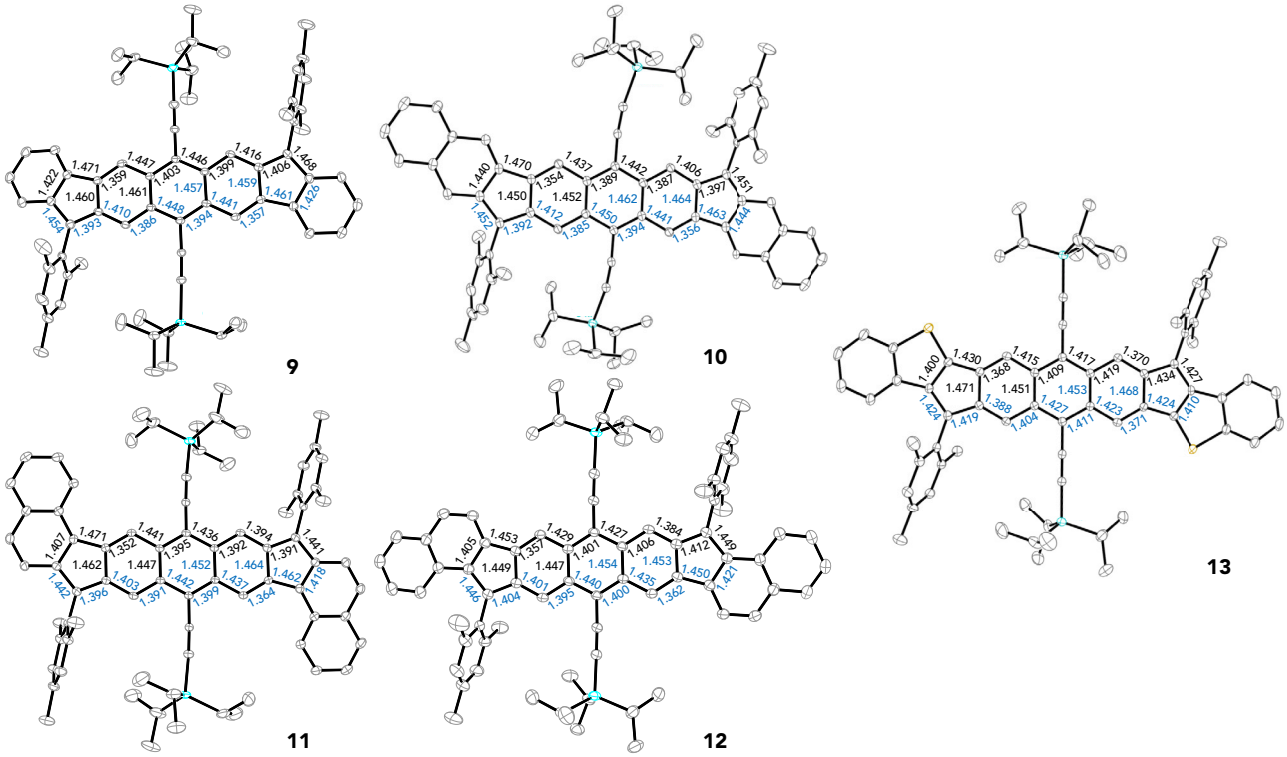

Figure 5. X-Ray Crystallographic Analysis of 9–13

X-ray structures of DIAn derivatives **10**–**13** with selected bond lengths (Å; experimental values in black and calculated values in blue) along with the previously published data for DIAn **9**; ellipsoids drawn at the 50% probability level. Experimental values for **12** and **13** are the average of the bond lengths found for the three and two symmetrically independent molecules, respectively.

Examination of the quinoidal core of **10**–**13** shows that the molecules possess bond lengths similar to those in the core of **9** (as might be expected) that range from 1.352 to 1.471 Å, and several of the quinoidal C=C bond lengths are near 1.4 Å. In particular, the bond length from the apical carbon of the five-membered ring carbon to the anthracene core is of great interest, as this can provide a first approximation of how open-shell a molecule is. This bond length in structurally analogous mesityl-substituted indenofluorene isomers can be as short as 1.380 Å in the closed-shell indeno[1,2-*b*]fluorene[23] and as long as 1.437 Å for proven open-shell indeno[2,1-*b*]fluorene,[24] which in the latter is accredited to the open-shell resonance form contributing more single bond character to this position as the diradical resonance form gains favor. In the case of PAHs **9**–**12**, these values run between 1.391–1.412 Å and is as large as 1.434 Å in **13**, suggesting that there are contributions from both the open-shell and the closed-shell resonance structures, corroborating the open-shell nature of these compounds. One might expect a trend of increasing bond length as the diradical character increases (**13** > **12** > **11** > **9** ≈ **10**). Although this expectation is supported by the calculated bond lengths as well as by the experimental values for four of the diareno-DIAns, isomer **11** is a notable exception, as it is the shortest of them all (1.391 Å), yet is calculated to be longer and more diradical than **9** or **10**.[62] It should be noted that the differences in the apical carbon bond lengths between **9**–**13** are close to the statistical margin of error of the XRD measurements, indicating that although a useful tool to gauge roughly how diradical a compound might be, this comparison is a "local" marker of the diradical character that does not consider the effect globally and is likely insufficient to account for small molecule-to-molecule variations in order to distinguish compounds with very similar diradical characters (e.g., **11** versus **12**).

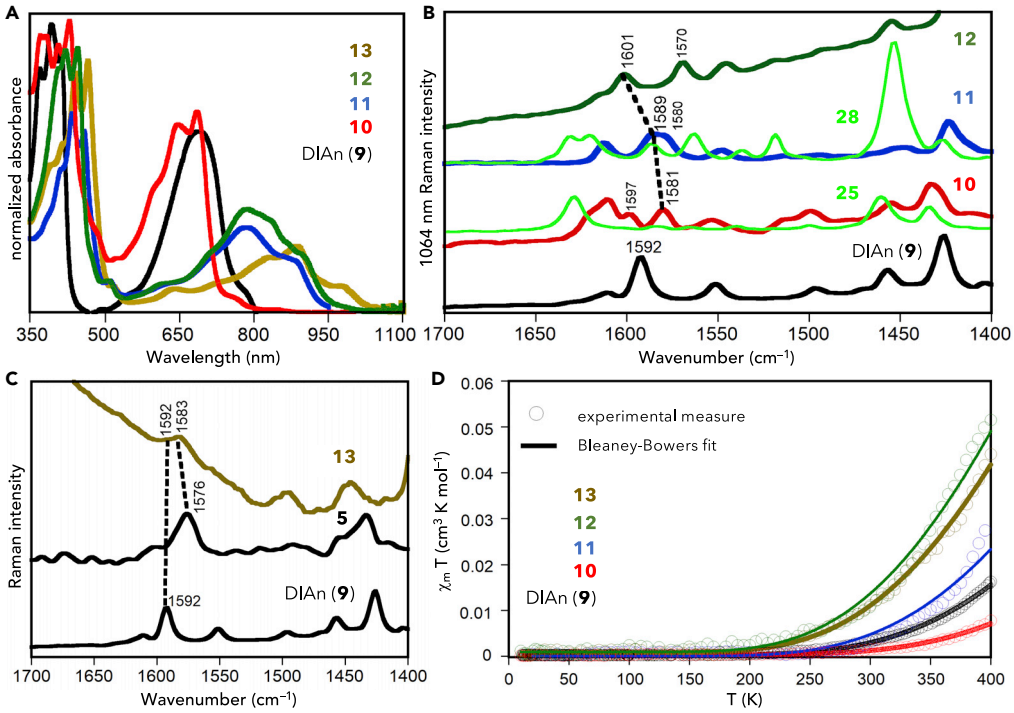

Figure 6. Spectroscopy and Magnetometry Data of 9–13

(A) Electronic absorption spectra of DIAn derivatives **9**–**13** in $CHCl_3$ solution at room temperature.

(B) Raman spectra of **9**–**12** and comparison with the dihydroDIAn precursors **25** and **28**.

(C) Raman spectra of **13** and comparison with **9** and the naphthalene core analog **5**.

(D) SQUID data of **9**–**13** in the solid state (empty circles) along with the corresponding Bleaney-Bowers fits (solid lines).

Electronic Absorption Spectroscopy

The diarenoDIAn derivatives **10**–**13** exhibit UV-vis-NIR electronic absorption spectra very similar to other related quinoidal polycyclic hydrocarbons and to the parent DIAn **9** (Figures 6A and S16). In addition, these spectra were recorded at low temperature (i.e., 80 K) in order to deal with those of the singlet ground electronic states, clean from triplet interference at 300 K (Figure S17 shows side-by-side comparison). Each spectrum displays characteristic absorptions of anthracene-based compounds showing electronic absorption in the range of 340–470 nm. Interestingly, in the low-energy region linear-**10** displays a slight blue-shifted absorption (700 nm) when compared with DIAn **9** (711 nm); however, there is a marked redshift on going from **10** to *syn*-**11** (803 nm), *anti*-**12** (839 nm), and **13** (955 nm), which is in agreement with the rather small change of the t_{ab} term on **9** → **10** and with the pronounced decrease of t_{ab} on going from **10** to **11**/**12** (see Table 1 and discussion thereof). The rich blue-green colors of **10**–**13** can be accredited to these low-energy absorptions that tail off into the near IR region (850–1,050 nm), because of the narrow HOMO-LUMO gap of these derivatives and are indicative of the large diradical contribution to the ground state. In addition, at lower energies, well-defined bands are recorded at 791 nm in **9**, 759 nm in **10**, 892 nm in **11**, 902 nm in **12**, and 1,044 nm in **13**, which behave in parallel to the main ones and that are explained as electronic absorptions arising from a low-lying doubly excited electronic configuration (Figure S17).[46–48] Interestingly, these bands, which usually appear as shoulders at room temperature, are clearly distinguished at 80 K. For completeness of the study, Figure S36 and Table S4 disclose the cyclic voltammetry electrochemical data also in comparison with that reported

for DIAn (**9**), which reveal very good agreement between the optically and electrochemically determined HOMO-LUMO energy gaps (1.13–1.41 eV) of **9**–**13**.

Raman Spectroscopy

To further track the changes in the molecule structure from the closed-shell to the open-shell resonance structures, Raman spectroscopy (Figure 6B) was performed on the three dibenzoDIAn derivatives and compared with the parent **9**. In regard of the interpretation of the significant variation of t_{ab} in this diradical series related with the tuned bonding of the two unpaired electrons through the central common anthracene spacer, the Raman spectra provide evidence of the vibrational structure of this central anthracene core. In the 1,550–1,600 cm^{-1} vibrational region in particular, the Raman bands associated with the collective C=C stretches of these central anthracene moieties appear, i.e., ν_{anth}(C=C). In Figures S37 and S38, theoretical Raman spectra are discussed, whereas Figure S39 shows the vibrational normal modes on which the assignment of the main Raman bands is based (see additional discussion in Section 10 of the Supplemental Information). In Figure 6B, we also show the Raman spectra of the dihydrogenated precursors of **10** and **11**, compounds **25** and **28**, respectively, which undoubtedly possess complete aromatic character in their anthracenes. On **25** → **10** and **28** → **11**, we observe downshifts of the ν_{anth}(C=C) wave number in agreement with the effect of partial quinoidization of these anthracenes (quinoidization always produces wave number downshifts).[20] According to this, the change between **28** and **11** ($\Delta\nu$ = 9 cm^{-1}) is smaller than between **25** and **10** ($\Delta\nu$ = 18 cm^{-1}) as a result of the larger diradical character (i.e., smaller quinoidal character) in **11**. For the series of diradical compounds under analysis, we observe that: (1) the ν_{anth}(C=C) wave number values of these bands differ from molecule to molecule and simultaneously, all these differ from that of DIAn **9**. (2) Among **10**/**11**/**12**, **10** appears at 1,581 cm^{-1}, the lowest wave number, revealing that of the three, this molecule keeps the larger degree of quinoidal character (i.e., consistent with the larger ΔE_{ST}). (3) From **11** to **12**, the difference of 12 cm^{-1} from 1,589 to 1,601 cm^{-1} is seemingly large but qualitatively consistent with ΔE_{ST}(**11**) > ΔE_{ST}(**12**). At the same time, this result is in agreement with the smaller ν_{anth}(C=C) differences between **28** and **11**, highlighting that the degree of aromaticity in the central anthracene in **12** is the largest among the three isomers and further corroborated by the smallest ΔE_{ST} found (*vide infra*).

Figure 6C also displays the Raman spectra of **13** compared with that of DIAn **9** and with the analogous benzothiophene-fused compound with a central naphthalene, i.e., molecule **5**. An upshift from **5** to **13** of the Raman band associated with the central moieties is detected, showing the larger overall aromaticity gained on the anthracene unit. On the other hand, comparing **13** and **9**, we observe the same ν_{anth}(C=C) wave number bands at 1,592 cm^{-1}, despite y (**9**) ≠ y (**13**), which is accounted by the particular U increasing role of the sulfur atoms, an electronic effect that in **9**/**13** does not essentially alter neither the bond length alternation pattern nor the vibrational pattern of the corresponding anthracenes.

Superconducting Quantum Interference Device Magnetometry

To experimentally examine the magnetic properties of this family of molecules with different computed singlet-triplet energy gaps, SQUID magnetometry was carried out. The magnetic behaviors up to 400 K were measured and the signals were subjected to a Bleaney-Bowers fitting[63] (Figure 6D) that only considers a dimer (low spin and high spin states) model. From these adjustments the ΔE_{ST} gaps were obtained and can be compared with the theoretically determined gaps in Table 1. The magnetic measurement is fully reversible, and the same curve can be reproduced in the

cooling direction back to room temperature (changes smaller than 5% of the total molar magnetic susceptibility before and after one cycle of heating-cooling), indicative of thermally resilient molecules. The absence of hysteresis in the heating and cooling curves shows that the routes for the population and depopulation of the high spin state do not differ. The resulting data also indicate that the ground electronic state is a singlet and the thermally excited state is a triplet, typical of molecules in which the diradical character is expressed by the correlation between the quinoidal and aromatic resonance forms. All of the newly determined ΔE_{ST} gaps are <10% variance from their calculated values. For example, the largest and smallest energy gaps are correctly measured and calculated for **10** ($\Delta E_{ST(exp)} = -4.8$, $\Delta E_{ST(calc)} = -5.09$ kcal mol^{-1}) and **12** ($\Delta E_{ST(exp)} = -3.2$, $\Delta E_{ST(calc)} = -3.45$ kcal mol^{-1}), respectively. Compounds **9**, **11**, and **13** also show very good agreement (Table 1). This narrow range of 1.6 kcal mol^{-1} for the experimental ΔE_{ST} values of the five molecules clearly supports our hypothesis of "fine-tuning" magnetic properties using a "structure refinement approach."

In conclusion, a new set of diradicaloid molecules based on the diindeno[1,2-*b*:1′,2′-*g*]anthracene motif has been prepared. A complete study addressing their spectroscopic and magnetic characterization together with model quantum chemical calculations has been carried out. Based on the 2 electron in 2 sites model, the diradical character is dictated by two electronic parameters, the repulsion term U and the transfer integral, t_{ab}. Here, we have shown how to design new diradicaloids based on the fine-tuning of the transfer integral term using structure refinement (altering external rings D and E in Figure 3) of a series of molecules containing a common 2,6-anthraceno conjugation of the two radical centers. Most notably, by making what might seem to be minor changes to the fusion "BO" of the outer rings, we were able to incrementally and rationally tune the singlet-triplet energy gap of the diarenoDIAn series over a narrow 1.6 kcal mol^{-1} range. As demonstrated by this study, we are aiming to produce real, synthesizable compounds illustrating how to exploit electronic structure concepts, such as U and t_{ab}. These structure-property connections and their complete understanding are mandatory for the rational design of diradicaloid molecules, i.e., diradicals with tailored singlet-triplet energy gaps for specific organic electronic applications.

EXPERIMENTAL PROCEDURES

Full experimental procedures are provided in the Supplemental Information.

DATA AND CODE AVAILABILITY

Crystallographic data have been deposited in the Cambridge Crystallographic Data Center (CCDC) under accession numbers CCDC: 1949611 (**17**), 1949612 (**11**), 1949613 (**10**), 1949614 (**12**), and 1964314 (**13**). These data can be obtained free of charge from the CCDC at http://www.ccdc.cam.ac.uk/data_request/cif.

SUPPLEMENTAL INFORMATION

Supplemental Information can be found online at https://doi.org/10.1016/j.chempr.2020.02.010.

ACKNOWLEDGMENTS

This work was supported by the US National Science Foundation (CHE-1565780), by the Spanish Government, MINECO (PGC2018-098533-B-100, CTQ2016-80955, and CTQ2017-87201-P), by Junta de Andalucía, Spain (UMA18FEDERJA057), the Japan Society for the Promotion of Science (JSPS, KAKENHI grants JP18H01943,

JP17H05157, and JP26107004), Kyoto Technoscience Center, and the Iketani Science and Technology Foundation. Mass spectrometry capabilities in the CAMCOR facility are supported by the NSF (CHE-1625529). Theoretical calculations were partly performed using Research Center for Computational Science, Okazaki, Japan.

AUTHOR CONTRIBUTIONS

J.J.D. and M.M.H. conceived the project. J.J.D., G.E.R., A.M.V., and B.E.C. designed and carried out the experiments. J.J.D. analyzed the data and wrote the manuscript. M.M.H. played a critical role in discussion of the experimental design, project direction, experiments and results, and preparation of the manuscript. L.N.Z. acquired and analyzed the X-ray crystallographic data. A.C.V. performed the Raman spectroscopic measurements. C.J.G.-G. acquired and interpreted the magnetic SQUID experiments. J.C. interpreted the spectroscopic data and co-wrote the paper. R.K. and M.N. performed the calculations on the geometry optimization, the open-shell character, and the ST gaps. All authors discussed the results and commented on the manuscript.

DECLARATION OF INTERESTS

The authors declare no competing interests.

Received: September 11, 2019
Revised: January 13, 2020
Accepted: February 14, 2020
Published: March 6, 2020

REFERENCES

1. For a review, see: Y Gopalakrishna, T., Zeng, W., Lu, X., and Wu, J. (2018). From open-shell singlet diradicaloids to polyradicaloids Chem. Commun (Camb). *54*, 2186–2199.

2. Morita, Y., Suzuki, S., Sato, K., and Takui, T. (2011). Synthetic organic spin chemistry for structurally well–defined open-shell graphene fragments. Nat. Chem. *3*, 197–204.

3. Morita, Y., Nishida, S., Murata, T., Moriguchi, M., Ueda, A., Satoh, M., Arifuku, K., Sato, K., and Takui, T. (2011). Organic tailored batteries materials using stable open-shell molecules with degenerate frontier orbitals. Nat. Mater. *10*, 947–951.

4. Nakano, M., Kishi, R., Nitta, T., Kubo, T., Nakasuji, K., Kamada, K., Ohta, K., Champagne, B., Botek, E., and Yamaguchi, K. (2005). Second hyperpolarizability (gamma) of singlet diradical system: dependence of gamma on the diradical character. J. Phys. Chem. A *109*, 885–891.

5. Nakano, M., Kishi, R., Ohta, S., Takahashi, H., Kubo, T., Kamada, K., Ohta, K., Botek, E., and Champagne, B. (2007). Relationship between third-order nonlinear optical properties and magnetic interactions in open-shell systems: a new paradigm for nonlinear optics. Phys. Rev. Lett. *99*, 033001.

6. Nakano, M., and Champagne, B. (2015). Theoretical design of open-shell singlet molecular systems for nonlinear optics. J. Phys. Chem. Lett. *6*, 3236–3256.

7. Hu, X., Wang, W., Wang, D., and Zheng, Y. (2018). The electronic applications of stable diradicaloids: present and future. J. Mater. Chem. C *6*, 11232–11242.

8. Minami, T., and Nakano, M. (2012). Diradical character view of singlet fission. J. Phys. Chem. Lett. *3*, 145–150.

9. Smith, M.B., and Michl, J. (2013). Recent advances in singlet fission. Annu. Rev. Phys. Chem. *64*, 361–386.

10. Varnavski, O., Abeyasinghe, N., Aragó, J., Serrano-Pérez, J.J., Ortí, E., López Navarrete, J.T., Takimiya, K., Casanova, D., Casado, J., and Goodson, T., III. (2015). High yield ultrafast intramolecular singlet exciton fission in a quinoidal bithiophene. J. Phys. Chem. Lett. *6*, 1375–1384.

11. Kioke, H., Chikamatsu, M., Azumi, R., Tsutsumi, J., Ogawa, K., Yamane, W., Nishiuchi, T., Kubo, K., Hasegawa, T., and Kanai, K. (2016). Stable delocalized singlet biradical hydrocarbon for organic field-effect transistors. Adv. Funct. Mater. *26*, 277–283.

12. Ni, Y., Lee, S., Son, M., Aratani, N., Ishida, M., Samanta, A., Yamada, H., Chang, Y.T., Furuta, H., Kim, D., and Wu, J. (2016). A diradical approach towards BODIPY-based dyes with intense near-infrared absorption around λ = 1100 nm. Angew. Chem. Int. Ed. Engl. *55*, 2815–2819.

13. Thiele, J., and Balhorn, H. (1904). Ueber einen chinoïden Kohlenwasserstoff. Ber. Dtsch. Chem. Ges. *37*, 1463–1470.

14. Tschitschibabin, A.E. (1907). Über einige phenylierte derivate des *p,p*-ditolyls. Ber. Dtsch. Chem. Ges. *40*, 1810–1819.

15. For a review, see: Abe, M. (2013). Diradicals Chem. Rev. *113*, 7011–7088.

16. Kubo, T., Shimizu, A., Sakamoto, M., Uruichi, M., Yakushi, K., Nakano, M., Shiomi, D., Sato, K., Takui, T., Morita, Y., and Nakasuji, K. (2005). Synthesis, intermolecular interaction, and semiconductive behavior of a delocalized singlet biradical hydrocarbon. Angew. Chem. Int. Ed. Engl. *44*, 6564–6568.

17. Shimizu, A., Kubo, T., Uruichi, M., Yakushi, K., Nakano, M., Shiomi, D., Sato, K., Takui, T., Hirao, Y., Matsumoto, K., et al. (2010). Alternating covalent bonding interactions in a one-dimensional chain of a phenalenyl-based singlet biradical molecule having Kekulé structures. J. Am. Chem. Soc. *132*, 14421–14428.

18. Shimizu, A., Hirao, Y., Matsumoto, K., Kurata, H., Kubo, T., Uruichi, M., and Yakushi, K. (2012). Aromaticity and π-bond covalency: prominent intermolecular covalent bonding interaction of a Kekulé hydrocarbon with very significant singlet biradical character. Chem. Commun. (Camb.) *48*, 5629–5631.

19. Kubo, T., Sakamoto, M., Akabane, M., Fujiwara, Y., Yamamoto, K., Akita, M., Inoue, K., Takui, T., and Nakasuji, K. (2004). Four-stage amphoteric redox properties and biradicaloid character of tetra-*tert*-butyldicyclopenta[*b;d*]thieno[1,2,3-*cd*;5,6,7-*c′d′*]diphenalene. Angew. Chem. Int. Ed. Engl. *43*, 6474–6479.

20. For a review, see: Casado, J. (2017). Para-quinodimethanes: a unified review of the

quinoidal-versus-aromatic competition and its implications Top. Curr. Chem. *375*, 73.

21. Zeng, Z., and Wu, J. (2015). Stable π-Extended p-quinodimethanes: synthesis and tunable ground states. Chem. Rec. *15*, 322–328.

22. Zeng, Z., Ishida, M., Zafra, J.L., Zhu, X., Sung, Y.M., Bao, N., Webster, R.D., Lee, B.S., Li, R.W., Zeng, W., et al. (2013). Pushing extended *p*-quinodimethanes to the limit: stable tetracyano-oligo(*N*-annulated perylene) quinodimethanes with tunable ground states. J. Am. Chem. Soc. *135*, 6363–6371.

23. Chase, D.T., Fix, A.G., Kang, S.J., Rose, B.D., Weber, C.D., Zhong, Y., Zakharov, L.N., Lonergan, M.C., Nuckolls, C., and Haley, M.M. (2012). 6,12-Diarylindeno[1,2-*b*]fluorenes: syntheses, photophysics, and ambipolar OFETs. J. Am. Chem. Soc. *134*, 10349–10352.

24. Shimizu, A., Kishi, R., Nakano, M., Shiomi, D., Sato, K., Takui, T., Hisaki, I., Miyata, M., and Tobe, Y. (2013). Indeno[2,1-*b*]fluorene: A 20-π-electron hydrocarbon with very low-energy light absorption. Angew. Chem. Int. Ed. Engl. *52*, 6076–6079.

25. Dressler, J.J., Zhou, Z., Marshall, J.L., Kishi, R., Takamuku, S., Wei, Z., Spisak, S.N., Nakano, M., Petrukhina, M.A., and Haley, M.M. (2017). Synthesis of the unknown indeno[1,2-a] fluorene regioisomer: crystallographic characterization of its dianion. Angew. Chem. Int. Ed. Engl. *56*, 15363–15367.

26. For a review see: Frederickson, C.K., Rose, B.D., and Haley, M.M. (2017). Explorations of the Indenofluorenes and expanded quinoidal analogues Acc. Chem. Res. *50*, 977–987.

27. Rudebusch, G.E., Zafra, J.L., Jorner, K., Fukuda, K., Marshall, J.L., Arrechea-Marcos, I., Espejo, G.L., Ponce Ortiz, R.P., Gomez-García, C.J., Zakharov, L.N., et al. (2016). Diindeno-fusion of an anthracene as a design strategy for stable organic biradicals. Nat. Chem. *8*, 753–759.

28. Rudebusch, G.E., Espejo, G.L., Zafra, J.L., Peña-Alvarez, M., Spisak, S.N., Fukuda, K., Wei, Z., Nakano, M., Petrukhina, M.A., Casado, J., and Haley, M.M. (2016). A biradical balancing act: redox amphoterism in a diindenoanthracene derivative results from quinoidal acceptor and aromatic donor motifs. J. Am. Chem. Soc. *138*, 12648–12654.

29. Marshall, J.L., Uchida, K., Frederickson, C.K., Schütt, C., Zeidell, A.M., Goetz, K.P., Finn, T.W., Jarolimek, K., Zakharov, L.N., Risko, C., et al. (2016). Indacenodibenzothiophenes: synthesis, optoelectronic properties and materials applications of molecules with strong antiaromatic character. Chem. Sci. *7*, 5547–5558.

30. Miyoshi, H., Miki, M., Hirano, S., Shimizu, A., Kishi, R., Fukuda, K., Shiomi, D., Sato, K., Takui, T., Hisaki, I., et al. (2017). Fluoreno[2,3-*b*] fluorene vs indeno[2,1-*b*]fluorene: unusual relationship between the number of π electrons and excitation energy in *m*-quinodimethane-type singlet diradicaloids. J. Org. Chem. *82*, 1380–1388.

31. Barker, J.E., Frederickson, C.K., Jones, M.H., Zakharov, L.N., and Haley, M.M. (2017). Synthesis and properties of quinoidal fluorenofluorenes. Org. Lett. *19*, 5312–5315.

32. Frederickson, C.K., Barker, J.E., Dressler, J.J., Zhou, Z., Hanks, E.R., Bard, J.P., Zakharov, L.N., Petrukhina, M.A., and Haley, M.M. (2018). Synthesis and characterization of a fluorescent dianthraceno-indacene. Synlett *29*, 2562–2566.

33. Dressler, J.J., Teraoka, M., Espejo, G.L., Kishi, R., Takamuku, S., Gómez-García, C.J., Zakharov, L.N., Nakano, M., Casado, J., and Haley, M.M. (2018). Thiophene and its sulfur inhibit indenoindenodibenzothiophene diradicals from low-energy lying thermal triplets. Nat. Chem. *10*, 1134–1140.

34. For a review, see: Hu, P., and Wu, J. (2017). Modern zethrene chemistry Can. J. Chem. *95*, 223–233.

35. Zeng, W., Sun, Z., Herng, T.S., Gonçalves, T.P., Gopalakrishna, T.Y., Huang, K.W., Ding, J., and Wu, J. (2016). Super-heptazethrene. Angew. Chem. Int. Ed. Engl. *55*, 8615–8619.

36. Sun, Z., Lee, S., Park, K.H., Zhu, X., Zhang, W., Zheng, B., Hu, P., Zeng, Z., Das, S., Li, Y., et al. (2013). Dibenzoheptazethrene isomers with different biradical characters: an exercise of Clar's aromatic sextet rule in singlet biradicaloids. J. Am. Chem. Soc. *135*, 18229–18236.

37. Li, Y., Heng, W.K., Lee, B.S., Aratani, N., Zafra, J.L., Bao, N., Lee, R., Sung, Y.M., Sun, Z., Huang, K.W., et al. (2012). Kinetically blocked stable heptazethrene and octazethrene: closed-shell or open-shell in the ground state? J. Am. Chem. Soc. *134*, 14913–14922.

38. For a review see: Konishi, A., Hirao, Y., Kurata, H., Kubo, T., Nakano, M., and Kamada, K. (2014). Anthenes: model systems for understanding the edge state of graphene nanoribbons Pure Appl. Chem. *86*, 497–505.

39. Konishi, A., Hirao, Y., Matsumoto, K., Kurata, H., Kishi, R., Shigeta, Y., Nakano, M., Tokunaga, K., Kamada, K., and Kubo, T. (2013). Synthesis and characterization of quarteranthene: elucidating the characteristics of the edge state of graphene nanoribbons at the molecular level. J. Am. Chem. Soc. *135*, 1430–1437.

40. Bendikov, M., Duong, H.M., Starkey, K., Houk, K.N., Carter, E.A., and Wudl, F. (2004). Oligoacenes: theoretical prediction of open-shell singlet diradical ground states. J. Am. Chem. Soc. *126*, 7416–7417.

41. Purushothaman, B., Bruzek, M., Parkin, S.R., Miller, A.F., and Anthony, J.E. (2011). Synthesis and structural characterization of crystalline nonacenes. Angew. Chem. Int. Ed. Engl. *50*, 7013–7017.

42. Dong, S., Gopalakrishna, T.Y., Han, Y., Phan, H., Tao, T., Ni, Y., Liu, G., and Chi, C. (2019). Extended bis(anthraoxa)quinodimethanes with nine and ten consecutively fused six-membered rings: neutral diradicaloids and charged diradical dianions/dications. J. Am. Chem. Soc. *141*, 62–66.

43. Kubo, T. (2015). Recent progress in quinoidal singlet biradical molecules. Chem. Lett. *44*, 111–122.

44. Sun, Z., Zeng, Z., and Wu, J. (2014). Zethrenes, extended *p*-quinodimethanes, and periacenes with a singlet biradical ground state. Acc. Chem. Res. *47*, 2582–2591.

45. Zeng, Z., Shi, X., Chi, C., López Navarrete, J.T., Casado, J., and Wu, J. (2015). Pro-aromatic and anti-aromatic π-conjugated molecules: an irresistible wish to be diradicals. Chem. Soc. Rev. *44*, 6578–6596.

46. Ravat, P., Šolomek, T., Ribar, P., and Juríček, M. (2016). Biradicaloid with a twist: lowering the singlet–triplet gap. Synlett *27*, 1613–1617.

47. Di Motta, S., Negri, F., Fazzi, D., Castiglioni, C., and Canesi, E.V. (2010). Biradicaloid and polyenic character of quinoidal oligothiophenes revealed by the presence of a low-lying double-exciton state. J. Phys. Chem. Lett. *1*, 3334–3339.

48. Sun, Z., Ye, Q., Chi, C., and Wu, J. (2012). Low band gap polycyclic hydrocarbons: from closed-shell near infrared dyes and semiconductors to open-shell radicals. Chem. Soc. Rev. *41*, 7857–7889.

49. Lu, R.Q., Wu, S., Yang, L.L., Gao, W.B., Qu, H., Wang, X.Y., Chen, J.B., Tang, C., Shi, H.Y., and Cao, X.Y. (2019). Stable Diindeno-fused corannulene regioisomers with open-shell singlet ground states and large diradical characters. Angew. Chem. Int. Ed. Engl. *58*, 7600–7605.

50. Zeng, W., Phan, H., Herng, T.S., Gopalakrishna, T.Y., Aratani, N., Zeng, Z., Yamada, H., Ding, J., and Wu, J. (2017). Rylene ribbons with unusual diradical character. Chem *2*, 81–92.

51. Yamaguchi, K. (1975). The electronic structures of biradicals in the unrestricted Hartree-Fock approximation. Chem. Phys. Lett. *33*, 330–335.

52. Frederickson, C.K., Zakharov, L.N., and Haley, M.M. (2016). Modulating Paratropicity strength in Diareno-fused antiaromatics. J. Am. Chem. Soc. *138*, 16827–16838.

53. Motomura, S., Nakano, M., Fukui, H., Yoneda, K., Kubo, T., Carion, R., and Champagne, B. (2011). Size dependences of the diradical character and the second hyperpolarizabilities in dicyclopenta-fused acenes: relationships with their aromaticity/antiaromaticity. Phys. Chem. Chem. Phys. *13*, 20575–20583.

54. Barker, J.E., Dressler, J.J., Cárdenas Valdivia, A.C., Kishi, R., Strand, E.T., Zakharov, L.N., MacMillan, S.N., Gómez-García, C.J., Nakano, M., Casado, J., and Haley, M.M. (2020). Molecule isomerism modulates the diradical properties of stable singlet diradicaloids. J. Am. Chem. Soc. *142*, 1548–1555.

55. Shao, Y., Head-Gordon, M., and Krylov, A.I. (2003). The spin–flip approach within time-dependent density functional theory: theory and applications to diradicals. J. Chem. Phys. *118*, 4807–4818.

56. Wang, F., and Ziegler, T. (2006). Use of noncollinear exchange-correlation potentials in multiplet resolutions by time-dependent density functional theory. Int. J. Quantum Chem. *106*, 2545–2550.

57. Iikura, H., Tsuneda, T., Yanai, T., and Hirao, K. (2001). A long-range correction scheme for generalized-gradient-approximation exchange functionals. J. Chem. Phys. *115*, 3540–3544.

58. Stein, T., Eisenberg, H., Kronik, L., and Baer, R. (2010). Fundamental gaps in finite systems from eigenvalues of a generalized Kohn-Sham method. Phys. Rev. Lett. *105*, 266802.

59. Park, J.H., Chung, D.S., Park, J.W., Ahn, T., Kong, H., Jung, Y.K., Lee, J., Yi, M.H., Park, C.E., Kwon, S.K., and Shim, H.K. (2007). Soluble and easily crystallized anthracene derivatives: precursors of solution-processable semiconducting molecules. Org. Lett. *9*, 2573–2576.

60. Nakagawa, H., Kawai, S., Nakashima, T., and Kawai, T. (2009). Synthesis and photochemical reactions of photochromic terarylene having a leaving methoxy group. Org. Lett. *11*, 1475–1478.

61. It is worth noting that we did explore use of other low-melting NMR solvents; however, 12 proved to be less soluble and/or precipitated from solution at very cold temperatures.

62. We repeated the X-ray determination of 11 with a crystal from a different batch of material yet obtained essentially the same bond length values.

63. Bleaney, B., and Bowers, K.D. (1952). Anomalous paramagnetism of copper acetate. Proc. R. Soc. Lond. A *214*, 451–465.